JOURNAL OF AIRCRAFT
Vol. 37, No. 3, May–June 2000

Eigenmode Analysis and Reduced-Order Modeling of Unsteady Transonic Potential Flow Around Airfoils

Razvan Florea,* Kenneth C. Hall,† and Earl H. Dowell‡
Duke University, Durham, North Carolina 27708-0300

An eigenmode analysis and reduced-order models of the unsteady transonic aerodynamic flow around isolated airfoils are presented. The unsteady flow is modeled using the time-linearized frequency-domain unsteady transonic full potential equation. The full potential was discretized in space using a finite element method. The resulting equations are linear in the unknown velocity potential and quadratic in the reduced frequency of excitation. The dominant eigenfrequencies and corresponding mode shapes of the discretized potential model are computed, and the effect of different parameters that determine the steady and unsteady flowfield (e.g., the far-field Mach number, the angle of attack, and the airfoil shape) are investigated. A normal mode analysis and a static correction technique are then used to construct a low degree-of-freedom, reduced-order model of the unsteady flowfield. Depending on the range of frequencies of interest, a relatively small number of eigenmodes are required. An alternative reduced-order modeling technique based on Arnoldi–Ritz vectors is also presented. For the case where the structural excitations are known a priori, the latter method is more efficient. Using the aerodynamic reduced-order models, we construct aeroelastic reduced-order models and compute flutter boundaries for different airfoils at several different Mach numbers.

Nomenclature

$\boldsymbol{A}_A$ = matrix operator for the Krylov/Arnoldi subspace
$\boldsymbol{A}_{0,1,2}$ = unsteady aerodynamic matrices
$\mathcal{A}$ = state-space form unsteady aerodynamic matrix
$\mathcal{A}_F$ = aeroelastic matrix
a = pitch axis location, normalized by semichord
$\mathcal{B}$ = state-space form unsteady aerodynamic matrix
$\mathcal{B}_F$ = aeroelastic matrix
b = semichord
$\boldsymbol{b}$ = frequency-independent vector, right-hand side of Eq. (8)
$\boldsymbol{b}_{0,1,2}$ = frequency-independent vectors, right-hand side of Eq. (7)
c = chord
c_l = linearized unsteady lift coefficient
c_{mea} = linearized unsteady moment coefficient about the elastic axis
$\boldsymbol{g}^{(N_c)}$ = participation factor in the solution with N_c static corrections, Eq. (11)
$\boldsymbol{H}^{(k)}$ = nonsymmetric upper Hessenberg matrix
h = plunge degree of freedom
$\boldsymbol{h}$ = airfoil displacement vector, $[h,\ \alpha]^T$
$\boldsymbol{I}_2$ = identity matrix of order 2
j = $\sqrt{-1}$
$\boldsymbol{K}$ = nondimensional elastic stiffness matrix
$\boldsymbol{M}$ = nondimensional mass matrix
N_c = number of static corrections
$\boldsymbol{q}$ = vector of generalized linearized unsteady aerodynamic forces, $[c_l,\ c_{\text{mea}}]^T$
r_α = radius of gyration, normalized by semichord
s = complex shift
$\boldsymbol{T}^{(k)}$ = upper triangular matrix at step k, Eq. (19)
$\boldsymbol{T}_{\text{hq}}^{0,1}$ = matrices relating airfoil motion $\boldsymbol{h}$ to generalized forces $\boldsymbol{q}$
$\boldsymbol{T}_{\phi q}^{0,1}$ = matrices relating vector potential ϕ to generalized forces $\boldsymbol{q}$
t = time
$\bar{u}$ = reduced velocity, $V_\infty/(b\omega_\alpha)$
$\boldsymbol{u}$ = state-space solution vector
$\boldsymbol{u}_D$ = dynamic part, state-space solution vector
$\boldsymbol{u}_S$ = static part, state-space solution vector
V_∞ = freestream velocity
$\boldsymbol{V}^{(k)}$ = orthonormal Arnoldi subspace
$x,\ y$ = Cartesian coordinates
x_α = static unbalance, normalized by semichord
$\boldsymbol{x}_i, \boldsymbol{y}_i$ = right and left eigenvectors
$z_i, \boldsymbol{Z}$ = eigenvector and matrix of eigenvectors of $\boldsymbol{H}^{(k)}$
α = pitching degree of freedom
θ = steady (mean) flow angle of attack
λ = eigenvalue, $j\omega$
λ_F = aeroelastic eigenvalue
μ = mass ratio, $m/(\pi\rho b^2)$
ν = artificial viscosity
ρ = static density
σ_i, Σ = eigenvalue, diagonal matrix of eigenvalues of $\boldsymbol{H}^{(k)}$
ϕ = velocity potential
ω = frequency, rad/s
$\bar{\omega}$ = reduced frequency, $\omega c/V_\infty$
ω_h = plunge natural frequency
ω_α = pitch natural frequency

I. Introduction

OVER the last decade, computational aerodynamic models of unsteady flows about airfoils and wings have become increasingly sophisticated and accurate. However, when used in aeroelastic analyses, such methods are extremely expensive. In most of these analyses, time-marching, time-accurate computational fluid dynamic codes are used. These models have several advantages: they are well developed and documented, straightforward to implement, and can be used in both linear and nonlinear analyses. Nevertheless, these computational models are not well suited to aeroelastic calculations because they require relatively small time steps and, therefore, require large amounts of CPU time. Furthermore, when repeated calculations are required, the analysis must be run repeatedly, increasing cost. For each new structural parameter, frequency, or mode shape of structural vibration, a complete new simulation

Presented at the CEAS/AIAA/ICASE/NASA Langley International Forum on Aeroelasticity and Structural Dynamics, Williamsburg, VA, 22–25 June 1999; received 12 July 1999; revision received 29 November 1999; accepted for publication 12 December 1999.

*Assistant Research Professor, Department of Mechanical Engineering and Materials Science. Member AIAA.

†Associate Professor, Department of Mechanical Engineering and Materials Science. Associate Fellow AIAA.

‡Professor, Department of Mechanical Engineering and Materials Science. Fellow AIAA.

is required. For a review of current trends in aeroelasticity we refer the reader to Refs. 1 and 2.

A first step in improving the computational efficiency of aeroelastic analyses is to use time-linearized unsteady models. In this approach, one assumes that the unsteady flowfield is decomposed into a mean (steady) flow and a small-disturbance unsteady flow. The resulting small-disturbance equations are time-invariant variable coefficient equations and can be formulated in either the time or frequency domain. One first solves for the nonlinear mean flow and then for the time-linearized unsteady flow. Although time-linearized models are computationally more efficient then time-nonlinear methods, they are subject to some of the same restrictions mentioned earlier when used for repeated computations with different parameters.

Recently, so-called reduced-order models[4] have been developed to improve further the efficiency of unsteady aerodynamic and aeroelastic analyses. Some of these techniques are well established in structural dynamics and, therefore, it seems natural to extend them to unsteady aerodynamics. In these methods, one reduces the large number of degrees-of-freedom unsteady aerodynamic model to a system with a much smaller number of states. At the same time, one wants to preserve the accuracy of the original model for some range of parameters, for example, over some range of frequencies of interest. Eigenmode-based reduced-order models for unsteady aerodynamic flows about airfoils, wings, and turbomachinery cascades have been constructed by Hall,[3] Florea and Hall,[4] Romanowski and Dowell,[5] and Florea et al.[6] Using this approach, the dominant eigenvectors of the linearized unsteady flows are computed, and then the unsteady flow solution is projected onto the space defined by these vectors. One or more static corrections are applied to improve the accuracy of the method.

Several other reduced-order modeling methods have been recently developed. Baker et al.[7] have applied internal balance reduction techniques to relatively simple two- and three-dimensional flows discretized with a vortex-lattice method. Although the results were promising, no complex unsteady flow model reductions were presented in Ref. 7.

More recently, reduced-order modeling technique based on proper orthogonal decomposition have been developed. Extensive reviews of this technique were published by Sirovich[8] and by Holmes et al.[9] Romanowski[10] has applied this method to create aeroelastic reduced-order models of time-linearized unsteady two-dimensional flows around isolated airfoils. Kim[11] used a similar approach to create reduced-order models of time-linearized, frequency-domain unsteady flows around a three-dimensional vortex-lattice model of a rectangular wing. At the same time, Hall et al.[12] constructed reduced-order models of time-linearized, frequency-domain unsteady flows around two-dimensional isolated airfoils and cascades.

In this paper, we present two reduced-order modeling techniques of small-disturbance, frequency-domain, unsteady transonic full-potential flows around isolated airfoils. First, an eigenmode analysis of the unsteady flow for several freestream Mach numbers, angles of attack, and airfoil shapes is performed. Then, we apply the concepts developed by Florea and Hall[4] to construct eigenmode-based reduced-order models of the unsteady transonic flow. We also present an alternative and more efficient reduction technique based on Arnoldi–Ritz vectors. The latter method is shown to be effective for the high subsonic and transonic regimes where the number of eigenmodes required in the eigenmode-based reduction is larger than the corresponding number of Arnoldi–Ritz vectors.

II. Nonlinear Mean Flow and Linearized Unsteady Flowfield Description

We consider the unsteady transonic flow around an isolated two-dimensional airfoil due to vibratory motion of the airfoil. The flow is assumed irrotational and isentropic, and thus only weak shocks are considered. Under these conditions, the unsteady transonic full-potential equation can be used to model the flowfield around the airfoil. The unsteady transonic full-potential equation is given by

$$\frac{\partial \hat{\rho}}{\partial t} + \nabla \cdot (\hat{\rho} \nabla \hat{\phi}) = 0 \tag{1}$$

where $\hat{\phi}$ is the velocity potential. The quantity $\hat{\rho}$ is the local density defined by the unsteady isentropic relation

$$\hat{\rho} = \rho_T \left\{ 1 - \frac{\gamma - 1}{\gamma} \frac{\rho_T}{p_T} \left(\frac{\partial \hat{\phi}}{\partial t} + \frac{1}{2} (\nabla \hat{\phi})^2 \right) \right\}^{1/(\gamma - 1)} \tag{2}$$

where ρ_T and p_T are the total density and total pressure (assumed to be constant throughout the entire field). Appropriate boundary conditions are used to enforce the airfoil surface impermeability condition, Kutta condition, and correct far-field behavior. Details of the flow linearization and discretization and of the boundary conditions for subsonic flows are given in Ref. 4.

A Galerkin finite element method with isoparametric quadrilateral bilinear elements is used to discretize the spatial derivatives of the flow equations and boundary conditions. This method is an extension of the variational finite element method developed by Hall for unsteady small-disturbance flows.[13] To improve the accuracy of the method, we use a strained coordinate system that moves with the airfoil near the airfoil and that is fixed in the far field. To produce the numerical dissipation necessary for the stability of supersonic flow solutions and to capture possible shocks, the local density in the divergence term of Eq. (1) is upwinded. Following Habashi and Hafez,[14] $\hat{\rho}_e$, the local density in the element e of the finite element discretization, is replaced by

$$\hat{\hat{\rho}}_e = \hat{\rho}_e - \hat{\nu}(\hat{\rho}_e - \hat{\rho}_{e-1}) \tag{3}$$

where $e - 1$ indicates the upstream element. The switching operator $\hat{\nu}$ is defined by Whitehead and Newton[15] as

$$\hat{\nu} = \nu_0 + (1 - 1/\hat{M}^2), \qquad \hat{M} \geq 1$$

$$\hat{\nu} = \nu_0 \hat{M}^{2/\nu_0} e^{-\nu_1 (\hat{M}-1)^2}, \qquad \hat{M} < 1 \tag{4}$$

with

$$\hat{M} = \max(\hat{M}_e, \hat{M}_{e-1}) \tag{5}$$

defining the local reference Mach number. The quantities ν_0 and ν_1 are constants with typical values $\nu_0 = 0.04$ and $\nu_1 = 20$.

A further simplification is made by assuming that the unsteadiness in the flow is small compared to the mean flow. This is consistent with the onset of flutter where the airfoil vibration and the resulting unsteady flow are small. The unsteady velocity potential and the moving grid are assumed to be harmonic in time, with frequency ω. For example,

$$\hat{\phi}(x, y) = \Phi(x, y) + \phi(x, y)\, e^{j\omega t} \tag{6}$$

where ϕ is the unsteady small-disturbance potential and Φ is the mean (steady) flow potential. Next, we time linearize the spatially discretized, unsteady full-potential system of equations. First, by collecting the zeroth-order terms from the linearization, we obtain a nonlinear system of equations that describes the mean flow. This system is just the discretization of the steady form of Eqs. (1–5) and the appropriate boundary conditions. Next, collecting the first-order terms from the linearization, we obtain a linear variable coefficient matrix equation for the unsteady small-disturbance flow in the frequency domain. The resulting discretized unsteady field equations and the corresponding boundary conditions have a quadratic form in the frequency domain ω, namely,

$$\left(\boldsymbol{A}_0 + j\omega \boldsymbol{A}_1 + \omega^2 \boldsymbol{A}_2\right)\phi = \boldsymbol{b}_0 + j\omega \boldsymbol{b}_1 + \omega^2 \boldsymbol{b}_2 \tag{7}$$

where the matrices $\boldsymbol{A}_0$, $\boldsymbol{A}_1$, and $\boldsymbol{A}_2$ are real nonsymmetric $n \times n$ matrices, and where n is the number of unknown entries in the vector ϕ. The matrices $\boldsymbol{A}_0$, $\boldsymbol{A}_1$, and $\boldsymbol{A}_2$ depend only on the nonlinear mean flow solution, while the vectors $\boldsymbol{b}_0$, $\boldsymbol{b}_1$, and $\boldsymbol{b}_2$ depend on both the mean flow solution and the prescribed motion of the airfoil.

We solve for the steady nonlinear mean flow solution using a direct Newton method. For the linearized unsteady equation, Eq. (7), the usual approach is to form the matrix coefficient $\boldsymbol{A}(\omega) = \boldsymbol{A}_0 + j\omega\boldsymbol{A}_1 + \omega^2\boldsymbol{A}_2$ for each frequency ω and mode of vibration (e.g., pitch or plunge) and then solve the resulting system using lower-upper (LU) decomposition. In the next section, we describe two alternative reduced-order modeling approaches.

III. Reduced-Order Modeling

A. Aerodynamic Reduced-Order Modeling Using Eigenmodes

An alternative approach for solving Eq. (7) is to use a normal mode analysis. First we observe that the right-hand side of Eq. (7) is a linear combination of the frequency-independent vectors $\boldsymbol{b}_0$, $\boldsymbol{b}_1$ and $\boldsymbol{b}_2$. Hence, one can solve Eq. (7) for each constant right-hand side vector $\boldsymbol{b}_i$ and then use the superposition method to obtain the solution of the original equation. To simplify our analysis, we assume that the right-hand side in Eq. (7) is a constant vector $\boldsymbol{b}$. Also, for convenience, we rewrite this equation in state-space form, that is,

$$\underbrace{\begin{pmatrix} \boldsymbol{G} & 0 \\ \boldsymbol{A}_1 & \boldsymbol{A}_0 \end{pmatrix}}_{\mathcal{A}} \underbrace{\begin{pmatrix} j\omega\phi \\ \phi \end{pmatrix}}_{\boldsymbol{u}} - j\omega \underbrace{\begin{pmatrix} 0 & \boldsymbol{G} \\ \boldsymbol{A}_2 & 0 \end{pmatrix}}_{\mathcal{B}} \underbrace{\begin{pmatrix} j\omega\phi \\ \phi \end{pmatrix}}_{\boldsymbol{u}} = \underbrace{\begin{pmatrix} \boldsymbol{0} \\ \boldsymbol{b} \end{pmatrix}}_{\bar{\boldsymbol{b}}} \tag{8}$$

where $\boldsymbol{G}$ is any nonsingular matrix. We first solve for the lower-frequency eigenvalues λ_i and the corresponding right and left eigenvectors, $\boldsymbol{x}_i$ and $\boldsymbol{y}_i$, of the homogeneous form of the matrix system Eq. (8), that is,

$$\mathcal{A}\boldsymbol{x}_i - \lambda_i\mathcal{B}\boldsymbol{x}_i = \boldsymbol{0}, \qquad \boldsymbol{y}_i^T\mathcal{A} - \lambda_i\boldsymbol{y}_i^T\mathcal{B} = 0 \tag{9}$$

To compute the eigenvalues and the corresponding eigenvectors numerically, one can use iterative Krylov techniques. We apply the non-symmetric Lanczos (see Ref. 16) and the block-Arnoldi (see Ref. 17) algorithms, both implemented to take into account the sparse, quadratic, generalized form of Eqs. (8) and (9).

Next, following Ref. 4, the unsteady solution is divided into two parts, a generalized static part $\boldsymbol{u}_S$, that does not depend on the eigenfrequencies and eigenmodes, but may depend on the frequency of excitation ω, and a generalized dynamic part $\boldsymbol{u}_D$, that depends on both the eigeninformation (eigenfrequencies and eigenmodes) and the frequency, that is,

$$\boldsymbol{u} = \underbrace{\sum_{k=1}^{N_c} (j\omega)^{k-1}\boldsymbol{u}_{S,k}}_{\boldsymbol{u}_S} + \underbrace{\sum_{i=1}^{m} g_i^{(N_c)}\boldsymbol{x}_i}_{\boldsymbol{u}_D} \tag{10}$$

where $g_i^{(N_c)}$ is the participation factor given by

$$g_i^{(N_c)} = (j\omega/\lambda_i)^{N_c}\left[\boldsymbol{y}_i^T\bar{\boldsymbol{b}}\Big/ (\lambda_i - j\omega)\right] \tag{11}$$

The static correction terms are defined by

$$\mathcal{A}\boldsymbol{u}_{S,1} = \bar{\boldsymbol{b}}, \qquad \mathcal{A}\boldsymbol{u}_{S,k} = \mathcal{B}\boldsymbol{u}_{S,k-1} \tag{12}$$

for $k > 1$. N_c is the number of static corrections and $m \ll 2n$ is the number of eigensolutions used in the modal expansion. We seek a solution ϕ given by Eqs. (10–12) that approximates the exact solution, the latter corresponding to $m = 2n$. That is, we want to reduce the contribution of the neglected modes without substantially increasing m. We can reduce the importance of each neglected mode by requiring that

$$|j\omega/\lambda_i|^{N_c} \ll 1 \tag{13}$$

for all of the neglected eigenmodes, $i > m$. Hence, we need to compute all of the eigenvalues and corresponding eigenmodes in the range of frequency of interest, and N_c should be as large as possible. However, the leading-order terms in each of the two series grow rapidly with increasing N_c. For large N_c, significant roundoff errors in the evaluation of the sum of two series in Eq. (13) occur and the method breaks down. We have found that good results are generally obtained for values of N_c between one and six (see Ref. 4 for details).

In the next section we will examine more closely the eigenvector solver as part of the reduced-order modeling technique and provide an alternative reduced-order model construction.

B. Aerodynamic Reduced-Order Modeling Using Arnoldi–Ritz Vectors

We use Krylov subspace methods to compute the eigenmodes of interest. These methods are efficient as long as the number of eigenfrequencies of interest is small. In such methods, starting with an initial arbitrary vector $\boldsymbol{W}_1$ and for the matrix operator $\boldsymbol{A}_A = \mathcal{A}^{-1}\mathcal{B}$, one computes iteratively a sequence of vectors, $\boldsymbol{W}_2 = \boldsymbol{A}_A\boldsymbol{W}_1$, $\boldsymbol{W}_3 = \boldsymbol{A}_A\boldsymbol{W}_2$, and so on, called Krylov vectors. These vectors form a subspace that approximates the subspace of dominant right eigenvectors of the eigenvalue problem defined by Eq. (9). We denote the matrix formed with the first k Krylov vectors by $\boldsymbol{W}^{(k)}$, that is,

$$\boldsymbol{W}^{(k)} = \left[\boldsymbol{W}_1 \mid \boldsymbol{A}_A\boldsymbol{W}_1 \mid \cdots \mid \boldsymbol{A}_A^{k-1}\boldsymbol{W}_1\right] \tag{14}$$

If we choose the initial vector $\boldsymbol{W}_1$ to be

$$\boldsymbol{W}_1 = \boldsymbol{u}_{S,1} = \mathcal{A}^{-1}\bar{\boldsymbol{b}} \tag{15}$$

then the static contribution in Eq. (10) $\boldsymbol{u}_S$ is just a linear combination of the columns of the Krylov matrix $\boldsymbol{W}^{(k)}$, that is,

$$\boldsymbol{u}_S = \boldsymbol{W}^{(k)}\Omega, \qquad \Omega = [1 \mid j\omega \mid \cdots \mid (j\omega)^{k-1}]^T \tag{16}$$

The Krylov iteration becomes unstable after a few steps, unless it is coupled with an orthonormalization process. For example, in the Arnoldi method, one starts with a unit vector $\boldsymbol{V}_1 = \boldsymbol{W}_1/\|\boldsymbol{W}_1\|_2$, and, at step k, the new vector $\boldsymbol{A}_A\boldsymbol{V}_{k-1}$ is first orthonormalized against previous vectors $\boldsymbol{V}_1$ to $\boldsymbol{V}_{k-1}$ before it is introduced as the new vector $\boldsymbol{V}_k$ in the sequence. These vectors are now called Arnoldi vectors and they form the $(2n \times k)$ orthonormal matrix $\boldsymbol{V}^{(k)}$ and satisfy the relation

$$\boldsymbol{H}^{(k)} = \boldsymbol{V}^{(k)H}\underbrace{(\mathcal{A}^{-1}\mathcal{B})}_{\boldsymbol{A}_A}\boldsymbol{V}^{(k)} \tag{17}$$

where $\boldsymbol{H}^{(k)}$ is a complex nonsymmetric upper Hessenberg matrix whose columns are easily computed during the Arnoldi iteration. The dominant eigenvalues of the matrix $\boldsymbol{A}_A$ are approximated by the dominant eigenvalues of the upper Hessenberg matrix $\boldsymbol{H}^{(k)}$. We denote by σ_i and z_i the ith largest eigenvalue and the corresponding eigenvector of the matrix $\boldsymbol{H}^{(k)}$, and λ_i and $\boldsymbol{x}_i$ are approximated by

$$\lambda_i \approx 1/\sigma_i, \qquad \boldsymbol{x}_i \approx \boldsymbol{V}^{(k)}z_i \tag{18}$$

Note that $\boldsymbol{V}^{(k)}$ and $\boldsymbol{W}^{(k)}$ span the same vector space and

$$\boldsymbol{W}^{(k)} = \boldsymbol{V}^{(k)}\boldsymbol{T}^{(k)} \tag{19}$$

where $\boldsymbol{T}^{(k)}$ is a $(k \times k)$ upper triangular matrix.

Taking into account Eqs. (10), (11), (16), (18), and (19), the reduced-order model solution can be written as a linear combination of the columns of $\boldsymbol{V}^{(k)}$, that is,

$$\boldsymbol{u} = \beta\boldsymbol{V}^{(k)}\left(\boldsymbol{Z}\boldsymbol{g} + \boldsymbol{T}^{(k)}\Omega\right), \qquad \beta = \|\boldsymbol{u}_{S,1}\|_2 \tag{20}$$

For known external excitations (airfoil motions), it is convenient to use $\boldsymbol{V}_1 = \boldsymbol{u}_{S,1}/\beta$ as the starting vector in the Arnoldi iteration without explicitly computing the eigenmodes defined by Eq. (9). This approach eliminates the need of a separate static correction step and greatly simplifies the reduced-order modeling algorithm. This method, a form of Ritz-based reduction, is similar to methods widely used in structural dynamics.[18,19]

Note that in the case of multiple right-hand side excitations (airfoil motions), the Krylov subspace iteration is replaced by a block-Krylov method.[17] For example, we consider the case of an isolated airfoil in pitch and plunge motion described by the airfoil displacement vector $\boldsymbol{h}$. We can write the Ritz–Arnoldi approximate solution as

$$\boldsymbol{u} = \boldsymbol{V}^{(k)}\boldsymbol{Z}\boldsymbol{u}_R \tag{21}$$

We substitute Eq. (21) into the original Eq. (8), we multiply at the left by $\mathcal{A}^{-1}$ and then by ${\boldsymbol{V}^{(k)}}^H$, and, taking into account the property stated in Eq. (17), we obtain

$$\boldsymbol{u}_R = (\boldsymbol{I} - j\omega\Sigma)^{-1} z^{-1}\beta \begin{bmatrix} \boldsymbol{I}_2 \\ j\omega\boldsymbol{I}_2 \\ \omega^2\boldsymbol{I}_2 \end{bmatrix} \boldsymbol{h} \tag{22}$$

where Σ is the diagonal matrix of the eigenvalues of $\boldsymbol{H}^{(k)}$. The orthonormal matrix $\boldsymbol{V}^{(k)}$ is determined iteratively during the block Arnoldi iteration with $\boldsymbol{V}_1$ being the starting block (matrix). The $(2n \times 6)$ matrix $\boldsymbol{V}_1$ and the (6×6) upper triangular matrix β are defined by the equation

$$\boldsymbol{V}_1 \underbrace{[\beta_0 \mid \beta_1 \mid \beta_2]}_{\beta} = \mathcal{A}^{-1} \underbrace{[\boldsymbol{b}_{0h}\ \boldsymbol{b}_{0\alpha}}_{\bar{\boldsymbol{b}}_0} \mid \underbrace{\boldsymbol{b}_{1h}\ \boldsymbol{b}_{1\alpha}}_{\bar{\boldsymbol{b}}_1} \mid \underbrace{\boldsymbol{b}_{2h}\ \boldsymbol{b}_{2\alpha}]}_{\bar{\boldsymbol{b}}_2} \tag{23}$$

where β_0, β_1, β_2 are now $(k \times 2)$ matrices, and $\bar{\boldsymbol{b}}_0$, $\bar{\boldsymbol{b}}_1$, and $\bar{\boldsymbol{b}}_2$ are $(2n \times 2)$ matrices.

Note that similar Ritz reduced-order models can be constructed around the Lanczos algorithm. For our analysis we found that the nonsymmetric Lanczos algorithm proved to be more reliable for eigenmode computations, whereas the block Arnoldi algorithm was more efficient for the direct Ritz reduction.

C. Flutter Analysis: Aeroelastic Reduced-Order Modeling

We consider here a two-degree-of-freedom airfoil. The structural dynamic equations in plunge and pitch can be written as

$$\left(-\omega^2 \overbrace{\begin{pmatrix} 1 & x_\alpha/2 \\ x_\alpha/2 & r_\alpha^2/4 \end{pmatrix}}^{M} + \omega_\alpha^2 \overbrace{\begin{pmatrix} (\omega_h/\omega_\alpha)^2 & 0 \\ 0 & r_\alpha^2/2 \end{pmatrix}}^{K}\right)\boldsymbol{h}$$

$$= (\omega_\alpha^2 \bar{u}^2/4)\boldsymbol{q} = \left(\boldsymbol{T}^0_{\phi q} + j\omega\boldsymbol{T}^1_{\phi q}\right)\phi + \left(\boldsymbol{T}^0_{\mathrm{hq}} + j\omega\boldsymbol{T}^1_{\mathrm{hq}}\right)\boldsymbol{h} \tag{24}$$

The matrices $\boldsymbol{T}^{0,1}_{\phi q}$ and $\boldsymbol{T}^{0,1}_{\mathrm{hq}}$ relate the potential vector ϕ and the airfoil motion $\boldsymbol{h}$ to the generalized forces $\boldsymbol{q}$ acting on the airfoil. These matrices are obtained by integrating the linearized unsteady pressure distribution over the airfoil. By combining the unsteady aerodynamic equations, Eq. (8), and the structural dynamic equations, Eq. (24), the aeroelastic eigenvalue equations in state-space form are obtained, that is,

$$\left(\overbrace{\left[\begin{array}{c|c|c} \mathcal{A} & -\bar{\boldsymbol{b}}_1 & -\bar{\boldsymbol{b}}_0 \\ 0 & \bar{\boldsymbol{I}}_2 & \bar{0} \\ -\boldsymbol{T}^0_{\mathrm{uq}} & -\boldsymbol{T}^1_{\mathrm{hq}} & \boldsymbol{K} - \boldsymbol{T}^0_{\mathrm{hq}} \end{array}\right]}^{\mathcal{A}_F} - \lambda_F \overbrace{\left[\begin{array}{c|c|c} \mathcal{B} & -\bar{\boldsymbol{b}}_2 & -0 \\ 0 & 0 & \boldsymbol{I}_2 \\ \boldsymbol{T}^1_{\mathrm{uq}} & -\boldsymbol{M} & 0 \end{array}\right]}^{\mathcal{B}_F}\right) \begin{bmatrix} \boldsymbol{u} \\ \lambda_F\boldsymbol{h} \\ \boldsymbol{h} \end{bmatrix} = \boldsymbol{0} \tag{25}$$

where the matrices

$$\boldsymbol{T}^0_{\mathrm{uq}} = \left[\boldsymbol{0} \mid \boldsymbol{T}^0_{\phi q}\right], \qquad \boldsymbol{T}^1_{\mathrm{uq}} = \left[\boldsymbol{0} \mid \boldsymbol{T}^1_{\phi q}\right] \tag{26}$$

relate the state-space vector $\boldsymbol{u}$ to the generalized forces $\boldsymbol{q}$ acting on the airfoil.

Note that the flutter matrices $\mathcal{A}_F$ and $\mathcal{B}_F$ are quite large, of order $(2n + 4)$, and depend on both aerodynamic and structural parameters. Using the Arnoldi–Ritz reduced-order aerodynamic solution, described by Eqs. (22) and (23), the eigenvalue problem Eq. (25) can be reduced to a much smaller reduced-order aeroelastic system of equations, that is,

$$\left(\left[\begin{array}{c|c|c} \boldsymbol{I}_k & -\beta_1 & -\beta_0 \\ 0 & \boldsymbol{I}_2 & \boldsymbol{0} \\ -\boldsymbol{T}^0_{\mathrm{uq}}\boldsymbol{V}^{(k)}\boldsymbol{Z} & -\boldsymbol{T}^1_{\mathrm{hq}} & \boldsymbol{K} - \boldsymbol{T}^0_{\mathrm{hq}} \end{array}\right] - \lambda_F \left[\begin{array}{c|c|c} \Sigma & -\beta_2 & -\boldsymbol{0} \\ \boldsymbol{0} & 0 & \boldsymbol{I}_2 \\ \boldsymbol{T}^1_{\mathrm{uq}}\boldsymbol{V}^{(k)}\boldsymbol{Z} & -\boldsymbol{M} & \boldsymbol{0} \end{array}\right]\right) \begin{bmatrix} \boldsymbol{u}_R \\ \lambda_F\boldsymbol{h} \\ \boldsymbol{h} \end{bmatrix} = \boldsymbol{0} \tag{27}$$

The aeroelastic reduced-order model can be used to compute the aeroelastic eigenvalues inside the domain of reduced frequencies where the aerodynamic reduced-order model is valid.

IV. Results

In this section, we present an eigenmode analysis and construct reduced-order models for unsteady flows around two isolated airfoils, a NACA 0012 symmetric airfoil and an MBB A3 nonsymmetric airfoil. We also compute flutter boundaries of the MBB A3 airfoil and NACA 64A010 (NASA Ames Research Center) airfoils for different Mach numbers. The computational grids used in all cases presented are O grids with a radius of 10 chords, with 129×51 mesh points (129 nodes around the airfoil and 51 nodes in the radial direction). A typical grid is shown if Fig. 1. This mesh point density is sufficient to ensure accurate steady solutions and unsteady solutions up to a reduced frequency of $\bar{\omega} = 2.0$.

A. Eigenspectrum

We first consider the steady and small perturbation unsteady flow around a NACA 0012 airfoil for several different Mach numbers and angles of attack. In each of these cases, we compute the eigenspectrum of the corresponding discretized unsteady potential flow. Shown in Fig. 2 is the eigenvalue distribution for the unsteady flow around a NACA 0012 airfoil for several different freestream Mach numbers M_∞ at zero angle of attack. For each of these cases we also show the steady Mach number distribution over the airfoil. For $M_\infty = 0.1$, the flow is, for all practical matters, incompressible. For $M_\infty = 0.7$, the flowfield is close to transonic, the highest local Mach number on the airfoil being 0.94. For $M_\infty = 0.85$, the flowfield becomes strongly transonic and the isentropic potential flow model is less accurate. Note that around the origin, the eigenspectrum is defined by lines of eigenvalues that emanate from the origin. These eigenvalues tend to be very close, and closer as the freestream Mach number increases. These lines of eigenvalues correspond to discrete representations of branch cuts.[4] In Fig. 3 we show the number of these eigenvalues around the origin, inside circles of radius 1.0 and 2.0, as a function of M_∞. Both Figs. 2 and 3 show that the density of the eigenspectrum changes significantly as the freestream Mach number increases from $M_\infty = 0.1$, corresponding to an incompressible regime, to $M_\infty = 0.7$, corresponding to a transonic regime. However, for the transonic regime, $M_\infty \geq 0.7$, the eigendistribution dependence on M_∞ becomes less sensitive.

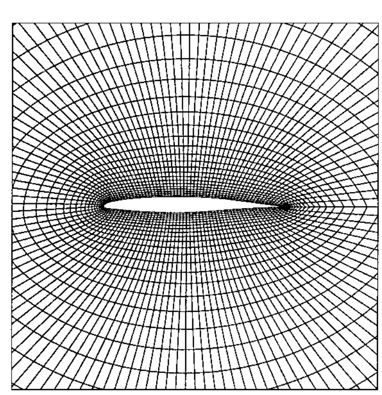

Fig. 1 Typical 129 × 51 node O grid around an MBB A3 isolated airfoil.

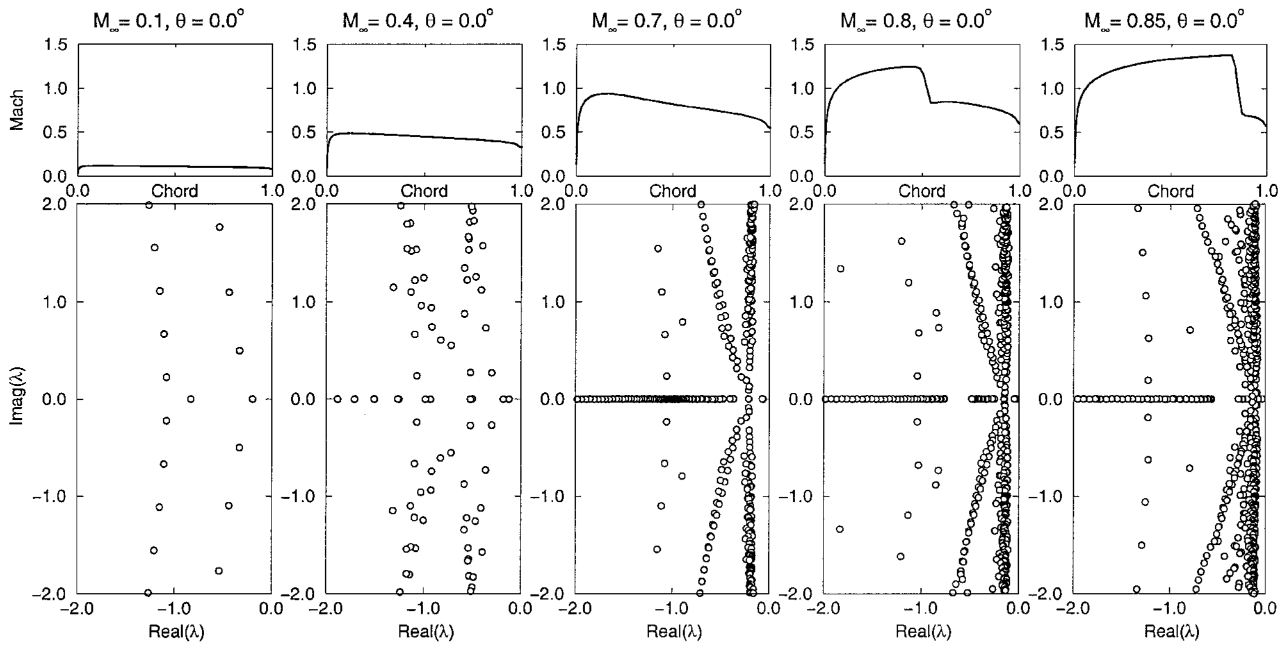

Fig. 2 Eigenvalues of unsteady flow about NACA 0012 airfoil for different Mach numbers at zero angle of attack.

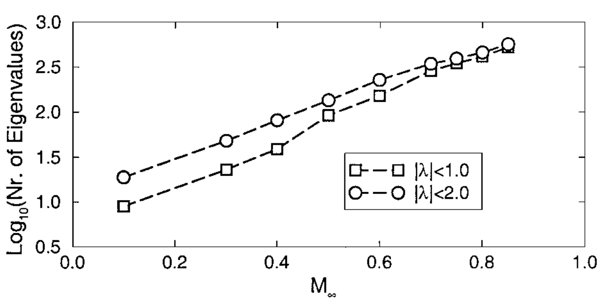

Fig. 3 Number of eigenvalues $|\lambda| < 1.0$ and $|\lambda| < 2.0$, of unsteady flow about NACA 0012 airfoil for different Mach numbers at zero angle of attack.

A few comments need to be made about the efficiency of the eigensolver. As Mach number increased, the eigenspectrum of the linearized unsteady flow became extremely dense and the Lanczos eigensolver failed to converge for a few of the eigenvalues around $\lambda = (-0.65, 0.0)$ in the complex plane. However, as we shall see, this does not affect the construction of the reduced-order model itself.

Shown in Fig. 4 is the effect of angle of attack on the eigenvalue distribution. As one can see, increasing the angle of attack has only a modest effect on the eigenvalue distribution, especially for the smaller eigenvalues, $|\lambda_i| < 0.6$. Also, the number of eigenvalues around the origin, $|\lambda| < 1.0$ and $|\lambda| < 2.0$, varies insignificantly (less then 1%) as the angle of attack is varied.

Next, we compute the eigenspectrum of the MBB A3 nonsymmetric airfoil for different angles of attack at the design Mach number, $M_\infty = 0.765$. The results are presented in Fig. 5. These results are consistent with the previous results for the symmetric NACA 0012 airfoil. Again, varying the angle of attack has only a modest effect of on the eigenvalue distribution. The number of eigenvalues around the origin, $|\lambda| < 1.0$ and $|\lambda| < 2.0$, shows a relatively small variation (less than 4%) and is about the same (within 8%) as for the NACA 0012 airfoil at the same Mach number. It also appears that the airfoil shape has little effect on the eigenspectrum distribution. All these results suggest that, for high subsonic flows and especially the transonic regime, the number of eigenvalues required for eigenmode-based reduction will be higher than for low subsonic flows.

B. Reduced-Order Models of Unsteady Flow

Using the dominant eigenvalues and eigenmodes of the unsteady flowfield around the MBB A3 airfoil, we constructed reduced-order models from which the unsteady pressure distribution due to airfoil motion can be computed. To increase the efficiency of the reduced-order model computation, namely, to reduce the number of eigenmodes required by Eq. (13), a shift s in the complex plane of the frequency domain was used. That is, in Eq. (7), the frequency ω was expressed in terms of the shifted frequency ω_s, defined by $j\omega_s = j\omega - s$. The unsteady potential equation, Eq. (7), than becomes

$$\left(\boldsymbol{A}_{0s} + j\omega_s \boldsymbol{A}_{1s} + \omega_s^2 \boldsymbol{A}_{2s}\right)\phi = \boldsymbol{b}_{0s} + j\omega_s \boldsymbol{b}_{1s} + \omega_s^2 \boldsymbol{b}_{2s} \tag{28}$$

where, for example,

$$\boldsymbol{A}_{0s} = \boldsymbol{A}_0 + s\boldsymbol{A}_1 - s^2\boldsymbol{A}_2 \tag{29}$$

Note that the quadratic form of Eq. (7) is maintained. Hence, the reduced-order modeling techniques presented in Sec. III can be applied to Eq. (28) with some minor modifications. That is, in the eigenmode analysis, the eigenmode-based and the Arnoldi–Ritz reduced-order models, the frequency ω, and the eigenvalues λ and λ_F are replaced by their corresponding shifted values. Then, Eq. (13) becomes

$$|(j\omega - s)/(\lambda_i - s)|^{N_c} \ll 1 \tag{30}$$

By carefully choosing the shift s, the required number of eigenvectors in the reduced-order modeling, given by Eq. (30), can be minimized.

We show in Fig. 6 the eigenmode selection for two reduced-order models, each using a different shift s. The first reduced-order model (ROM1) uses all of the 109 eigenvalues and corresponding eigenmodes inside a circle centered at $s = (0.0, 0.5)$ with a radius of 0.8. These 109 eigenmodes correspond to 1.6% of the total number of degrees of freedom (entries in the unknown vector ϕ). With five static corrections, this model should be valid for a range of reduced frequencies $0 \le \bar{\omega} \le 1$. For the second reduced-order model (ROM2), we choose the shift to be $s = (0.75, 1.0)$. By selecting the shift point s to be in the right-half plane, Eq. (30) allows us to select only the most important eigenmodes, that is, those that are lightly damped and therefore strongly excited by the harmonic excitations within the described frequency range. The included eigenvalues lie mainly in the first branch close to the vertical axis. We use all of the 237

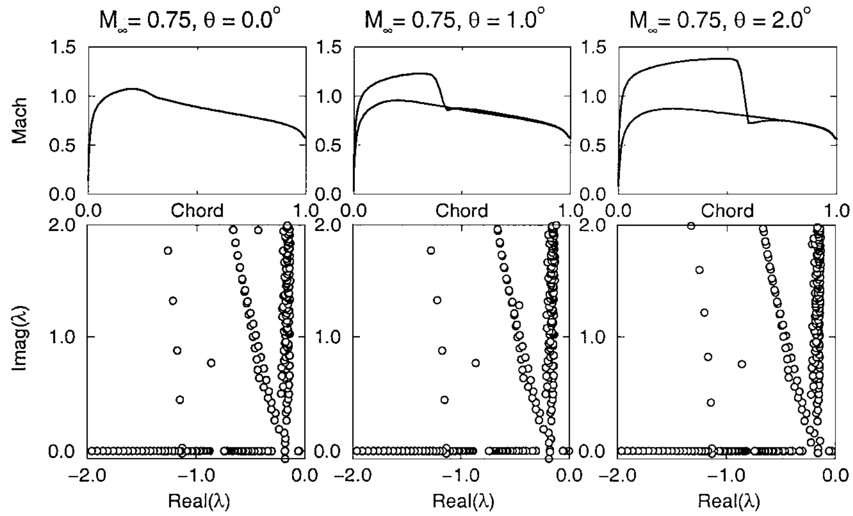

Fig. 4 Eigenvalues of unsteady flow about NACA 0012 airfoil at different angles of attack, M_∞ = 0.75.

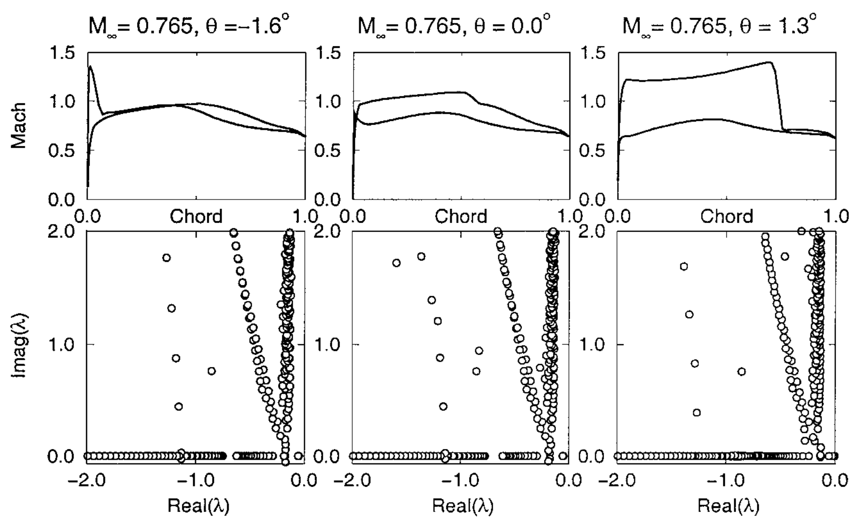

Fig. 5 Eigenvalues of unsteady flow about MBB A3 airfoil at different angles of attack, M_∞ = 0.765.

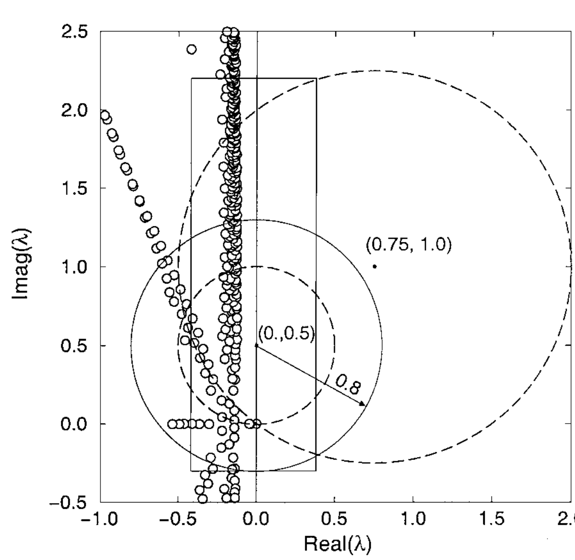

Fig. 6 Eigenmode selection for two reduced-order models of unsteady flow about MBB A3 airfoil: ——, eigenvalues included in reduced-order models; - - -, domain of validity of reduced-order models; mean flow conditions: $\theta = -0.5$ deg, and M_∞ = 0.79.

eigenmodes inside the rectangular box shown in Fig. 6. With five static corrections, this model should be valid for a range of frequencies $0 \le \bar{\omega} \le 2$ and uses only 3.6% of the total number of degrees of freedom. Shown in Fig. 7 is the unsteady lift computed using direct calculation and two reduced-order models defined by the two shifts and several static corrections. Both models are accurate in each of their predicted range of frequencies.

A few remarks are in order about the computational efficiency of the reduced-order models presented. For ROM1, the time to compute the eigenmodes and then to construct the reduced order model is about 12 times one direct calculation, whereas for ROM2 the factor rises to about 40 times. Note that once the eigenmodes have been computed, however, the unsteady aerodynamic response over a range of frequencies and structural mode shapes of vibration can be obtained for almost no additional cost.

For the same airfoil and flow conditions, namely the MBB A3 airfoil pitching about quarter chord, at $\theta = -0.5$ deg and $M_\infty = 0.79$, we have also used the Arnoldi–Ritz reduction technique to construct reduced-order models. We show in Fig. 8 the unsteady lift computed using this approach. Two reduced-order models are considered: one with 37 states and a more accurate one with 73 states. These correspond to 0.55% and 1.1% of the total number of degrees of freedom (entries in the unknown vector ϕ). For both Arnoldi–Ritz models, we choose a shift $s = (0.5, 0.5)$. The shifting technique ensures a better convergence to the unsteady flow solution (with no static

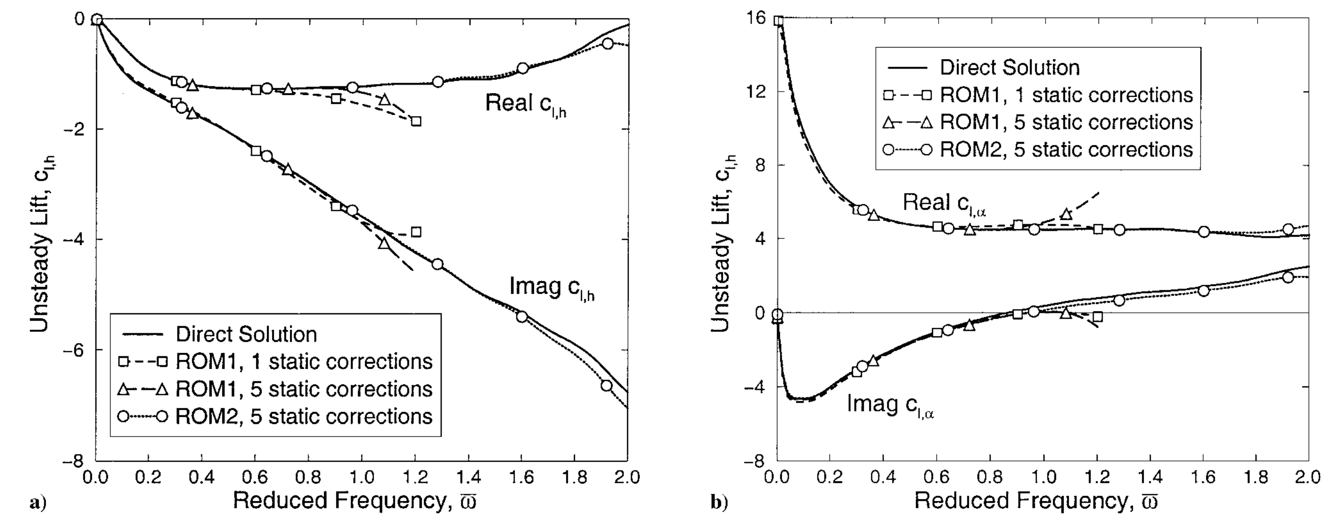

Fig. 7 Unsteady lift on MBB A3 airfoil pitching about quarter chord; mean flow conditions: $\theta = -0.5$ deg and $M_\infty = 0.79$; eigenmode-based reduced-order models, a) lift due to plunging, and b) lift due to pitching.

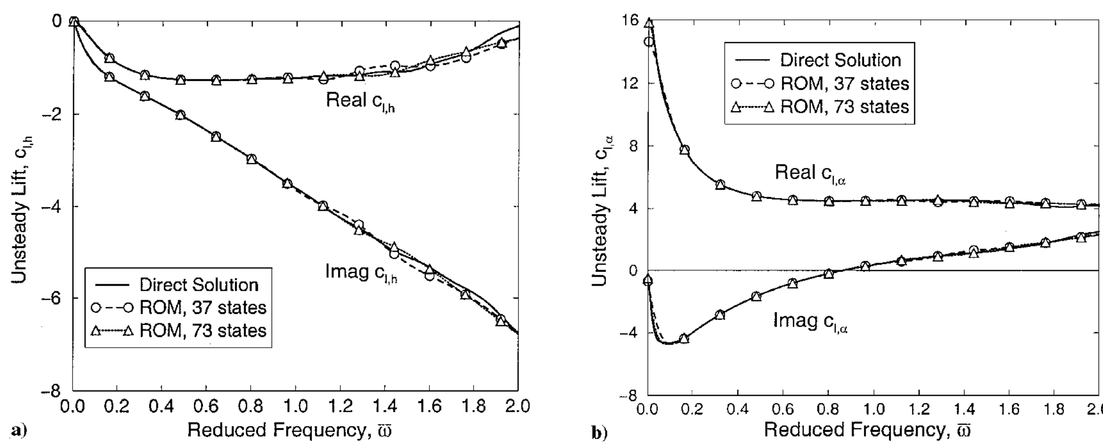

Fig. 8 Unsteady lift on MBB A3 airfoil pitching about quarter chord; mean flow conditions: $\theta = -0.5$ deg and $M_\infty = 0.79$; Ritz–Arnoldi reduced-order models, a) lift due to plunging, and b) lift due to pitching.

corrections) at the price of a poorer representation of the eigenspectrum of the unsteady flow. The computational time required to compute the Arnoldi–Ritz vectors and the reduced-order models are about two times one direct calculation for the first model and about four times for the second model. Both models are valid for a range of reduced frequencies $0 \leq \bar{\omega} \leq 2$ and are more accurate than the previous eigenmode based reduction models, but require an order of magnitude less computational time and a smaller number of states.

C. Flutter Analysis

We use the Arnoldi–Ritz reduction technique to compute the flutter boundaries for the MBB A3 airfoil and the NASA Ames Research Center design of the NACA 64A010 airfoil (called 64AMES herein). Both airfoils are described in Ref. 20. Calculations were made for each airfoil at different Mach numbers and one mean angle of attack: $\theta = -0.5$ deg for the MBB A3 airfoil and $\theta = 1.0$ deg for the 64AMES airfoil. The structural parameters, described in Ref. 21, are $a = -2$, $x_\alpha = 1.8$, $r_\alpha{}^2 = 3.48$, $\mu = 60$, and $\omega_h / \omega_\alpha = 1.0$.

First, we consider the MBB A3 airfoil at $M_\infty = 0.79$ and $\theta = -0.5$ deg. We show in Fig. 9 the root locus of the aeroelastic eigenvalues for different reduced velocities $\bar{u} = V_\infty / (b\omega_\alpha)$ computed with two different reduced-order models. In the first model, we use 37 states (Arnoldi vectors), whereas for the second model we use a much larger number of states, 181 vectors. For comparison we also

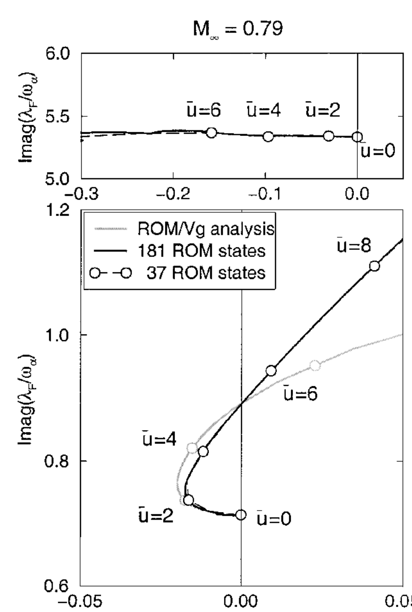

Fig. 9 Root locus of aeroelastic eigenvalues of MBB A3 airfoil computed with two Arnoldi–Ritz reduced-order models: $M_\infty = 0.79$, $\theta = -0.5$ deg.

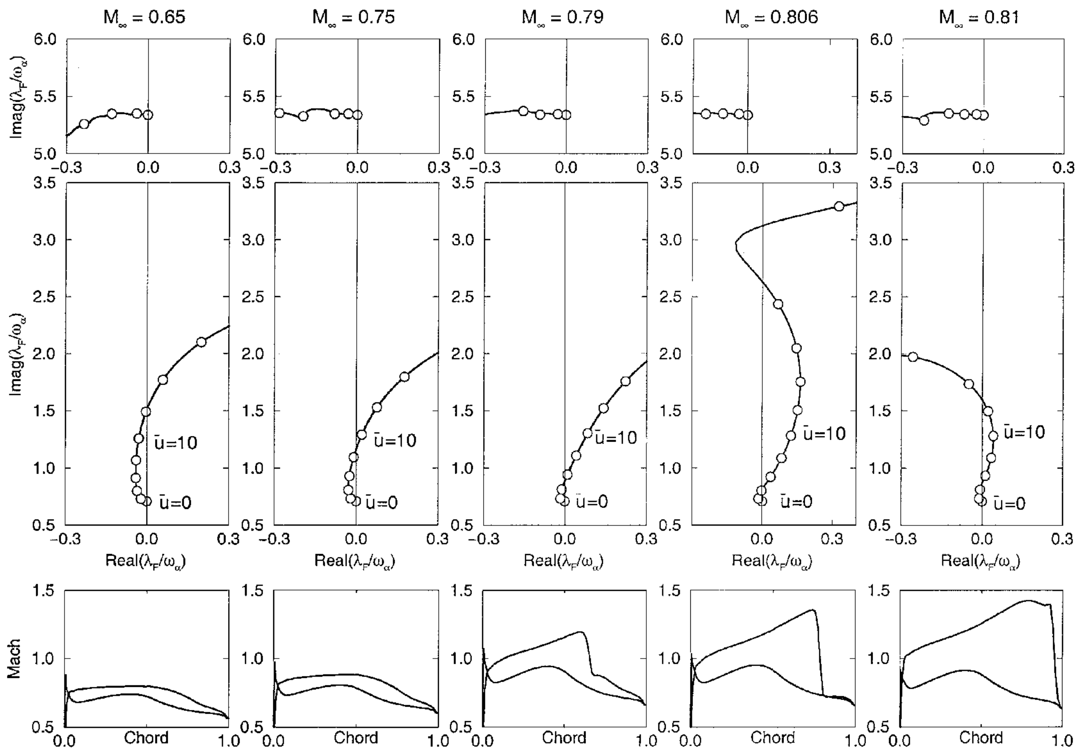

Fig. 10 Root locus of aeroelastic eigenvalues of MBB A3 airfoil computed with Arnoldi–Ritz reduced-order models (37 states): $\theta = -0.5$ deg.

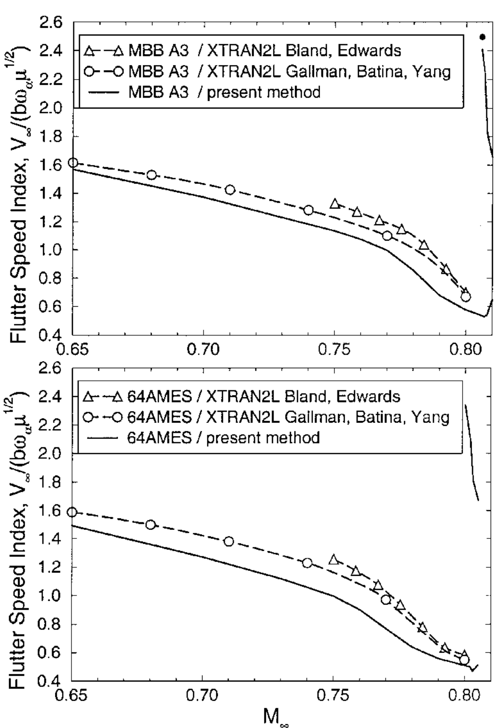

Fig. 11 Flutter boundaries for MBB A3 airfoil at $\theta = -0.5$ deg and 64AMES at $\theta = 1.0$ deg computed with transonic full-potential/Arnoldi–Ritz reduction technique (present method).

show the corresponding eigenvalue ratio $\lambda_{V_g}/\omega_\alpha$ calculated with the classical V–g analysis, that is,

$$\left(\lambda_{V_g} \middle| \omega_\alpha\right)^{-2} = (\omega_\alpha / j\omega)^2 (1 + jg) \tag{31}$$

where g is the required structural damping for neutral stability.[22] For the case presented in Fig. 9, we assumed no structural damping, $g_{\text{available}} = 0$. The corresponding V–g curve has physically meaningful values only when it crosses the vertical axis at $\bar{u} = 0$ (no wind) and at the flutter boundary $\bar{u} \neq 0$. Note that the curves based on aeroelastic reduced-order models are almost indistinguishable and all of the three models predict the same flutter boundary within 0.1% accuracy.

Next, we compute the root locus of aeroelastic eigenvalues for different Mach numbers at the same incidence $\theta = -0.5$ deg. Results are shown in Fig. 10. Similar calculations were done for the 64AMES airfoil at $\theta = 1.0$ deg. The flutter boundaries for the two airfoils are shown in Fig. 11. Note that all our results were calculated holding the mean angle θ fixed. This would correspond to a different static twist and a different nominal angle of attack at each point on the flutter curve. For comparison we also show the results obtained under the same assumption (of fixed mean angle) by Bland and Edwards[21] and by Gallman et al.[23] with XTRAN2L, transonic small perturbation theory.

Although the two sets of results are qualitatively the same, there are some quantitative differences, and these differences extend even into the compressible subsonic regime. These differences are mainly because for the same steady flow conditions, the present full-potential model predicts higher steady loads than the one reported in Refs. 21 and 23, especially for the MBB A3 airfoil. Similar mean steady flow pressure distribution differences for the MBB A3 airfoil were also reported in Ref. 24. Note that we were able to capture the minimum flutter speed index and the forming of a second branch of the flutter boundary around $M_\infty = 0.80$. However, above $M_\infty = 0.81$, the shock becomes much stronger and attached to the trailing edge, and the transonic full-potential model failed to converge when computing the steady flow.

V. Conclusions

Two reduced-order modeling techniques for analyzing small-disturbance, frequency-domain, unsteady transonic full-potential flows around isolated airfoils have been presented. First, we have performed an extensive eigenmode analysis of the discretized unsteady flow equations. This analysis showed that eigenspectrum density and distribution changes rapidly as the freestream Mach number increases from the subsonic incompressible regime to the incipient transonic regime. In the transonic regime, the eigendistribution is less sensitive to variation in freestream Mach number. Once the eigenvalues and and corresponding eigenmodes have been computed, reduced-order models of the unsteady flows were computed. The solution was divided into a dynamic part represented by a linear combination of the eigenmodes plus one or more static corrections. To reduce further the number of eigenmodes required in the model reduction, a shifting strategy based on the eigenspectrum distribution was employed. Depending on the range of frequencies of interest, the eigenmode-based reduction can be an efficient approach, even for the transonic regime. However, for the transonic regime, the computational time required to compute the eigenmodes is much higher than for the low compressible regime.

We have also implemented a second reduction technique based on the Arnoldi–Ritz vectors themselves. In the block-Arnoldi iteration, we used as starting vectors the vectors that define particular right-hand side solutions of the linearized unsteady flow equation. Then, during the Arnoldi iteration, we constructed an orthonormal basis of vectors with which we represent the unsteady flowfield solution. Our results show that although both eigenmode-based and Arnoldi–Ritz reduction methods are computationally efficient, the simplified Arnoldi-Ritz approach of using right-hand side information to construct reduced-order models is almost an order of magnitude more efficient. Using the aerodynamic reduced-order models, we have constructed aeroelastic reduced-order models that are easy to use in aeroelastic parametric studies. Flutter boundaries for different airfoils at several different Mach numbers have been computed. Finally, we note that the form the Arnoldi–Ritz reduced-order model is well suited for the study of active control of aeroelastic and aeroacoustic phenomena.

References

[1]Bennett, R. M., and Edwards, J. W., "Overview of Recent Developments in Computational Aeroelasticity," AIAA Paper 98-2421, June 1998.

[2]Friedmann, P. P., "Renaissance of Aeroelasticity and Its Future," *Journal of Aircraft*, Vol. 36, No. 1, 1999, pp. 105–121.

[3]Hall, K. C., "Eigenanalysis of Unsteady Flows About Airfoils, Wings, and Cascades," *AIAA Journal*, Vol. 32, No. 12, 1994, pp. 2426–2432.

[4]Florea, R., and Hall, K. C., "Eigenmode Analysis of Unsteady Flows About Airfoils," *Journal of Computational Physics*, Vol. 147, No. 2, 1998, pp. 568–593.

[5]Romanowski, M. C., and Dowell, E. H., "Reduced-Order Euler Equations for Unsteady Aerodynamic Flows: Numerical Techniques," AIAA Paper 96-0528, Jan. 1996.

[6]Florea, R., Hall, K. C., and Cizmas, P. G. A., "Eigenmode Analysis of Unsteady Viscous Flows in a Turbomachinery Cascades," *Unsteady Aerodynamics and Aeroelasticity of Turbomachines. Proceedings of the 8th International Symposium*, edited by T. H. Fransson, Kluwer Academic Publishers, Dordrecht, The Netherlands, 1998, pp. 767–782.

[7]Baker, M. L., Mingori, D. L., and Goggin, P. J., "Approximate Subspace Iteration for Constructing Internally Balanced Reduced-Order Models Of Unsteady Aerodynamic Systems," AIAA Paper 96-1441-CP, Presented at the AIAA/ASME/ASCE/ AHS/ASC 37th Structures, Structural Dynamics, and Materials Conf., Salt Lake City, UT, April 1996.

[8]Sirovich, L., "Turbulence and Dynamics of Coherent Structures. Part I: Coherent Structures. Part II: Symmetry and Transformations. Part III: Dynamics and Scaling," *Quarterly of Applied Mathematics*, Vol. 45, No. 3, 1987, pp. 561–590.

[9]Holmes, P., Lumley, J. L., and Berkooz, G., *Turbulence, Coherent Structures, Dynamical Systems and Symmetry*, Cambridge Univ. Press, Cambridge, England, U.K., 1996, pp. 86–128.

[10]Romanowski, M. C., "Reduced-Order Unsteady Aerodynamic and Aeroelastic Models Using Karhunen–Loève Eigenmodes," AIAA Paper 96-3981, Sept. 1996.

[11]Kim, T., "Frequency-Domain Karhunen–Loève Method and its Applications to Linear Dynamic Systems," *AIAA Journal*, Vol. 36, No. 11, 1998, pp. 2117–2123.

[12]Hall, K., Thomas, J. P., and Dowell, E. H., "Reduced-Order Modeling of Unsteady Small-Disturbance Flows Using a Frequency-Domain Proper Orthogonal Decomposition Technique," AIAA Paper 99-065, Jan. 1999, *AIAA Journal* (submitted for publication).

[13]Hall, K. C., "Deforming Grid Variational Principle for Unsteady Small Disturbance Flows in Cascades," *AIAA Journal*, Vol. 31, No. 5, 1993, pp. 891–900.

[14]Habashi, W. G., and Hafez, M. M., "Finite Element Solutions of Transonic Flow Problems," *AIAA Journal*, Vol. 20, No. 10, 1982, pp. 1368–1376.

[15]Whitehead, D. S., and Newton, S. G., "A Finite Element Method for the Solution of Two-Dimensional Transonic Flows in Cascades," *International Journal for Numerical Methods in Fluids*, Vol. 5, No. 2, 1985, pp. 115–132.

[16]Cullum, J., Kerner, W., and Willoughby, R., "A Generalized Nonsymmetric Lanczos Procedure," *Computer Physics Communications*, Vol. 53, No. 19, 1989, pp. 19–48.

[17]Saad, Y., *Numerical Methods for Large Eigenvalue Problems*, Manchester Univ. Press, Manchester, England, U.K., 1992, pp. 156–162, 186–194.

[18]Wilson, E. L., Yuan, M. W., and Dickens, J. M., "Dynamic Analysis by Direct Superposition of Ritz Vectors," *Earthquake Engineering and Structural Dynamics*, Vol. 10, No. 6, 1982, pp. 813–821.

[19]Noor, A. K., "Recent Advances and Applications of Reduction Methods," *Applied Mechanics Reviews*, Vol. 47, May 1994, pp. 125–145.

[20]Bland, S. R., "AGARD Two-Dimensional Aeroelastic Configurations," Advisory Rept. 156, AGARD, Aug. 1979.

[21]Bland, S. R., and Edwards, J. W., "Airfoil Shape and Thickness Effects on Transonic Airloads and Flutter," *Journal of Aircraft*, Vol. 21, No. 3, 1984, pp. 209–217.

[22]Dowell, E. H. (ed.), Crawley. E. F., Curtiss, H. C., Peters, D. A., Scanlan, R. H., and Sisto, F., *A Modern Course in Aeroelasticity*, 3rd rev. and enlarged ed., Kluwer Academic Publishers, Dordrecht, The Netherlands, 1995, pp. 106–118.

[23]Gallman, J. W., Batina, J. T., and Yang, T. Y., "Computational Transonic Flutter Boundary Tracking Procedure," AIAA Paper 86-902, May 1986.

[24]Zimmermann, H., "The Application of Transonic Unsteady Methods for Calculation of Flutter Airloads," *Transonic Unsteady Aerodynamics and Its Aeroelastic Applications*, CP-374, AGARD, 1984.